

1 **ENSO and MJO Modulation of U.S. Cloud-to-ground Lightning Activity**

2 Kelsey Malloy,^a Michael K. Tippett,^a William J. Koshak^b

3 ^a *Department of Applied Physics and Applied Mathematics, Columbia University, New York, New*
4 *York*

5 ^b *Earth Science Branch, NASA Marshall Space Flight Center, Huntsville, Alabama*

6 *Corresponding author: Kelsey Malloy, kmm2374@columbia.edu*

7 ABSTRACT: Cloud-to-ground (CG) lightning substantially impacts human health and property.
8 However, the relations between U.S. lightning activity and the Madden-Julian Oscillation (MJO)
9 and El Niño-Southern Oscillation (ENSO), two predictable drivers of global climate variability,
10 remain uncertain, in part because most lightning datasets have short records that cannot robustly
11 reveal MJO- and ENSO-related patterns. To overcome this limitation, we developed an empirical
12 model of 6-hourly lightning flash count over the contiguous U.S. (CONUS) using environmental
13 variables (convective available potential energy and precipitation) and National Lightning Detection
14 Network data for 2003–2016. This model is shown to reproduce the observed daily and seasonal
15 variability of lightning over most of CONUS. Then, the empirical model was applied to construct
16 a proxy lightning dataset for the period 1979–2021, which was used to investigate the summer
17 MJO-lightning relationship at daily resolution and the winter-spring ENSO-lightning relationship
18 at seasonal resolution. Overall, no robust relationship between MJO phase and lightning patterns
19 was found when seasonality was taken into consideration. El Niño is associated with increased
20 lightning activity over the Coastal Southeast U.S. during early winter, the Southwest during winter
21 through spring, and the Northwest during late spring, whereas La Niña is associated with increased
22 lightning activity over the Tennessee River Valley during winter.

23 SIGNIFICANCE STATEMENT: Cloud-to-ground lightning is dangerous for humans via direct
24 strikes or through triggering wildfires, generating air pollution, etc. How lightning activity can
25 be affected by climate remains unclear, and it is challenging to study their links because the data
26 record for lightning is short. With the available lightning record, we developed a model that relates
27 lightning flash counts over U.S. to environmental factors. This model well represents observed
28 fluctuations in daily and seasonal lightning over most of the U.S. Because the model only needs
29 environmental information to predict lightning flash counts, we were able to construct a longer
30 record of predicted lightning based on the longer data record of environmental variables. With
31 this dataset, we investigated the links between lightning and climate and found that the state of sea
32 surface temperatures in the tropical Pacific (El Niño-Southern Oscillation) is linked to changes in
33 U.S. lightning patterns in winter and spring.

34 **1. Introduction**

35 Cloud-to-ground (CG) lightning has large impacts on ecosystem health as well as human life
36 and property (Koshak et al. 2015). In particular, CG lightning is a natural trigger for wildfires
37 and can generate ground-level nitrogen oxides that lead to the production of tropospheric ozone
38 (Kang et al. 2020). More generally, lightning characteristics, such as flash rate and polarity, have
39 been linked to thunderstorm formation and structure (Goodman and MacGorman 1986; Branick
40 and Doswell III 1992) as well as severe weather events, such as hail and tornadoes (MacGorman
41 and Burgess 1994).

42 Although lightning has substantial impacts, relatively little is understood about its relation to
43 large-scale climate variability. For instance, only a few studies have investigated the relationship
44 between lightning and the El Niño-Southern Oscillation (ENSO), which is the dominant mode of
45 predictable climate variability on seasonal and interannual timescales. Dowdy (2016) showed a
46 statistical relation between ENSO and seasonal lightning activity in over 20% of the region 35°S–
47 35°N in some seasons, and Muñoz et al. (2016) used ENSO and other sea surface temperature
48 (SST) patterns to predict seasonal lightning activity in North Western Venezuela. LaJoie and Laing
49 (2008) and Laing et al. (2008) found a spatially sporadic winter ENSO-lightning relationship over
50 the Gulf Coast with an increase of lightning activity during El Niño in an 8-year dataset (1995–
51 2002). Koehler (2020) also found a positive relation between El Niño and U.S. lightning activity

52 in a 26-year dataset (1993–2018). However, their use of an annual (January–December) ENSO
53 index and contiguous U.S. (CONUS) totals precluded the resolution of spatial and temporal details
54 of the ENSO-lightning relationship and mixed ENSO states from one winter to the next. Overall,
55 an ENSO influence on U.S. lightning activity is plausible since ENSO explains a considerable
56 proportion of U.S. precipitation variability (L’Heureux et al. 2015; Nigam and Sengupta 2021) and
57 has been found to modulate the frequency of hail and tornadoes in winter and spring (Allen et al.
58 2015b; Koch et al. 2021; Tippett and Lepore 2021).

59 Likewise, few studies have examined the relation between lightning activity and the Madden-
60 Julian Oscillation (MJO), which is the dominant mode of predictable climate variability on sub-
61 seasonal timescales. Lightning density in MJO-associated tropical mesoscale convective systems
62 evolves with MJO life cycle (Virts and Houze 2015). Abatzoglou and Brown (2009) linked June–
63 September anomalous lightning activity to MJO phase in a 18-year dataset (1990–2007). Once
64 again, modulation of U.S. lightning activity by the MJO is plausible since the MJO modulates
65 U.S. precipitation (Becker et al. 2011) and may modulate spring and summer tornado activity
66 (Thompson and Roundy 2013; Baggett et al. 2018; Kim et al. 2020), though this relationship is
67 less robust than the ENSO-tornado relationship (Tippett 2018; Moore and McGuire 2020).

68 A challenge in investigating the relation between lightning and climate is that the ideal tools for
69 studying climate relations — observational data and physics-based models — have their limitations.
70 Lightning datasets often are relatively short or inhomogeneous, making it difficult to identify
71 significant relationships between lightning activity and climate modes of variability as well as to
72 discern trends due to a changing climate (Romps et al. 2014; Romps 2019; Finney et al. 2018). The
73 most realistic physics-based representations of lightning are those used for weather, not climate
74 timescales. In convection-permitting models, lightning is often parameterized based on cloud
75 dynamics and microphysics (Price and Rind 1994; Michalon et al. 1999; Mansell et al. 2005;
76 McCaul et al. 2009; Yair et al. 2010; Lynn et al. 2012; Fierro et al. 2013). However, these model
77 simulations tend to be relatively short with few ensemble members, making it difficult to extract a
78 robust ENSO or MJO signal in lightning activity compared to the model-based studies for ENSO-
79 or MJO-modulated temperature and precipitation patterns.

80 Empirical models provide an alternative approach by predicting lightning characteristics based
81 on environmental factors (Romps et al. 2014; Stolz et al. 2017). Romps et al. (2014) developed

82 a simple lightning proxy based on the product of convective available potential energy (CAPE),
83 precipitation, and a scaling factor. This CAPE times precipitation (CP) proxy is attractive for
84 many reasons. CAPE and precipitation are readily available in many reanalysis products and
85 forecast/climate models (Saha et al. 2014; Vitart et al. 2017; Lepore et al. 2018; Pegion et al.
86 2019), and both CAPE (Jung and Kirtman 2016) and precipitation (Becker et al. 2014; DelSole
87 et al. 2017) are forecasted with some skill on long-range timescales. Despite its simplicity, the
88 CP proxy represents subseasonal CG lightning activity fairly well (Tippett and Koshak 2018).
89 In addition, there is theoretical basis for how CAPE and precipitation might be modulated on
90 various timescales. Also, the relationships between lightning, CAPE, and precipitation are well
91 documented (Petersen and Rutledge 1998; Murugavel et al. 2012; Xu et al. 2013). For example,
92 Romps et al. (2014) and Murugavel et al. (2012) estimated future increasing lightning trends in
93 climate projections, using the corresponding CAPE and precipitation projections to explain these
94 trends.

95 Yet the CP proxy has substantial limitations. While its simple calculation is attractive for practical
96 purposes, a proportionality constant is the only tunable parameter. The CP proxy cannot capture
97 land-ocean lightning contrasts (Romps et al. 2018), attesting to its missing physical processes.
98 Consequently, its ability to capture CG lightning variability differs by region and season. For
99 example, Tippett et al. (2019) analyzed CP proxy performance in representing CG lightning
100 climatology and variability and found that CP proxy performance declined west of the Rocky
101 Mountains and during the summer season. Other studies that analyzed the CP proxy in other
102 regions of the world found that its performance varied by region or season, e.g., it under-performed
103 during Indian monsoon season relative to the pre-monsoon season (Dewan et al. 2018) and under-
104 performed in the plateau region of southwest China relative to other terrains (Zhao et al. 2022).
105 However, the CP proxy may still be a useful tool when and where its performance is adequate.

106 The purposes of this study are to (1) develop a CG lightning proxy that generalizes its functional
107 dependence on CAPE and precipitation, (2) evaluate the performance in capturing observed light-
108 ning variability on daily and seasonal timescales during the 2003–2016 period, and (3) demonstrate
109 use of the CG lightning proxy in assessing the influence of climate variability on CG lightning
110 activity during the longer 1979–2021 period. The data and methods used for constructing the
111 lightning proxy and conducting the remaining analysis are detailed in Section 2. In Section 3,

112 the results are presented in three parts. First, the new lightning proxy is compared to lightning
113 observations and the CP proxy for the 2003–2016 period. Then, two applications of the lightning
114 proxy are explored: 1979–2021 daily proxy data is used to analyze the MJO-lightning relationship
115 in summer, and 1979–2021 seasonal proxy data is used to analyze the ENSO-lightning relationship
116 in winter through late spring. These example applications complement previous work using shorter
117 records of lightning observations (e.g. Abatzoglou and Brown 2009; LaJoie and Laing 2008; Laing
118 et al. 2008). The longer lightning proxy could provide further insight into these relationships. In ad-
119 dition, this analysis provides information about the potential for lightning prediction on long-range
120 timescales from MJO and ENSO, two major sources of predictability on subseasonal-to-seasonal
121 timescales. A summary of the results as well as a discussion of its connection to findings from
122 previous literature and future work needed are given in Section 4.

123 **2. Data and Methods**

124 *a. Data*

125 CG lightning flash count data are taken from the National Lightning Detection Network (NLDN)
126 for the 2003–2016 period during which the network is reliable and there are few missing days
127 (Cummins and Murphy 2009; Koshak et al. 2015). There are nine days without data, which are
128 excluded from analysis, and there is a notable increase in lightning counts during 2016 that may
129 be from a change in the NLDN Total Lightning Processor (Nag et al. 2016). Lightning counts are
130 summed over CONUS land for every 6 hours (at 00, 06, 12, and 18 UTC) and at a $1^\circ \times 1^\circ$ grid
131 resolution. We use the total number of CG flashes, which is the sum of negative polarity flashes and
132 positive polarity flashes with currents greater than 15 kA. The positive polarity threshold accounts
133 for cloud pulses that are frequently misclassified as low-amplitude, positive CG lightning (Biagi
134 et al. 2007; Cummins and Murphy 2009).

135 Mixed-layer CAPE (J kg^{-1}) and precipitation (mm day^{-1}) data are taken from North American
136 Regional Reanalysis (NARR) for the 1979–2021 period (Mesinger et al. 2006). NARR provides
137 data at a 3-hour resolution with 32-km native grid spacing, which we convert to a 6-hour and
138 $1^\circ \times 1^\circ$ resolution. Mixed-layer CAPE in NARR is calculated from the mean equivalent potential
139 temperature between the 0–180 hPa layer. Because NARR assimilates latent heating profiles,
140 precipitation is better estimated in NARR than other global reanalyses (Bukovsky and Karoly

141 2007; Cui et al. 2017). Despite noted deficiencies of CAPE values in reanalysis (Gensini et al.
 142 2014), CAPE biases are smaller in NARR than other reanalysis products (King and Kennedy 2019).

143 MJO is defined by the real-time multivariate (RMM) index (Wheeler and Hendon 2004), which
 144 uses the normalized combined empirical orthogonal function (EOF) of outgoing longwave radia-
 145 tion, 200-hPa zonal wind, and 850-hPa zonal wind between 15°S–15°N to construct eight phases
 146 of the MJO. We only consider active MJO phases when the RMM amplitude is greater than or
 147 equal to 1.

148 ENSO is defined by the Oceanic Niño Index (ONI). ONI is taken from the Climate Prediction
 149 Center and is computed by averaging the SST anomalies over the Niño 3.4 region (5°N–5°S,
 150 120°–170°W), and a 3-month running mean is applied. El Niño is defined by an ONI greater than
 151 or equal to 0.5°C, and La Niña is defined by an ONI less than or equal to -0.5°C.

152 *b. Poisson Regression*

153 We fit the 6-hourly CG lightning flash counts for the 2003–2016 period using a Poisson regression
 154 (PR). In the PR model, the probability of the 6-hourly lightning flash count N taking on the values
 155 $n = 0, 1, 2, \dots$ is:

$$P(N = n) = \frac{e^{-\mu} \mu^n}{n!}, \quad (1)$$

156 where μ is the expected value of N . The expected value μ depends log-linearly on the vector \mathbf{x} of
 157 environmental predictors:

$$\mu \sim \exp(\mathbf{b}^T \mathbf{x}), \quad (2)$$

158 where \mathbf{b} is the vector of corresponding regression coefficients. The regression coefficients are
 159 estimated by maximizing the log-likelihood from Eq. 1 of the observed lightning flash counts given
 160 the environmental variables. Here, the sample size is 3,676,016 which is the number of land grid
 161 points times the number of 6-hourly periods during 2003–2016. We include an intercept term b_0
 162 in the regression as well as an offset term which accounts for the different areas of the 1°x1° grid
 163 boxes. Therefore, the expected lightning flash count μ in a grid box and within a 6-hourly interval
 164 is:

$$\mu = \exp[b_0 + \mathbf{b}^T \mathbf{x} + \log(\Delta \text{lat} \Delta \text{lon} \cos \phi)] \quad (3)$$

165 where Δlat and Δlon are the longitude and latitude spacings in degrees (both here are 1), respectively,
166 and ϕ is the latitude.

167 Three functional forms for the dependence of μ on precipitation and CAPE are tested. PR
168 Model 1 uses $\log(\text{CAPE} \times \text{Precipitation})$ as its predictor variable. PR Model 2 uses $\log(\text{CAPE})$
169 and $\log(\text{Precipitation})$ as its predictor variables. PR Model 3 uses $\log(\text{CAPE})$, $\log(\text{Precipitation})$,
170 $(\log(\text{CAPE}))^2$, and $(\log(\text{Precipitation}))^2$ as its predictor variables. The three models are nested in
171 the sense that PR Model 3 is a special case of PR Model 2, and PR Model 2 is special case of PR
172 Model 1, which facilitate their comparison. Using $\log(\text{CAPE})$ and $\log(\text{Precipitation})$ as predictors
173 means that μ has the following functional forms:

$$\text{PR Model 1: } \mu \sim (\text{CAPE} \times \text{Precipitation})^{b_1}$$

$$\text{PR Model 2: } \mu \sim (\text{CAPE})^{b_1} (\text{Precipitation})^{b_2}$$

$$\text{PR Model 3: } \mu \sim (\text{CAPE})^{b_1} (\text{Precipitation})^{b_2} \exp[b_3(\log(\text{CAPE}))^2 \\ + b_4(\log(\text{Precipitation}))^2]$$

174 where $\mathbf{b} = \{b_1, b_2, \dots\}$ are the corresponding coefficients for each predictor. We calculate deviance
175 to determine goodness of fit, with a smaller deviance indicating a better fit. We perform leave-
176 one-year-out jackknife resampling to quantify the uncertainty in the estimates of the regression
177 coefficients. For example, we leave out 2003 and estimate the PR coefficients with the 2004–2016
178 data, then leave out 2004 and estimate the PR coefficients with the 2003 and 2005–2016 data,
179 and so on. We use the 2.5 and 97.5 percentile of the resulting coefficients as 95% confidence
180 intervals. The spatial and temporal rank correlations between observed and predicted flash counts
181 are computed to evaluate performance.

182 After selecting and fitting a PR model, CAPE and precipitation data from 1979–2021 are used
183 in the PR model as a proxy for 6-hourly lightning flash counts, which are aggregated to daily and
184 seasonal resolution. For the MJO analysis, we calculate flash anomaly composites. For the ENSO
185 analysis, we calculate the rank correlation between the 3-month running season flash anomaly (daily
186 mean removed) and ONI. In addition, difference composites of lightning flashes are computed,
187 which is the average of the lightning flashes during El Niño subtracted from the average of the
188 lightning flashes during La Niña.

189 *c. Statistical Significance*

190 A bootstrapping test (with replacement) is used to assess the statistical significance of the temporal
191 rank correlations.

192 A Wilcoxon rank sum test is used to assess the statistical significance of the difference between
193 El Niño and La Niña composites. The Wilcoxon rank sum test procedure is non-parametric i.e.,
194 does not assume known distribution and essentially compares the medians of the composited sets.

195 We use a two-sided permutation test that preserves day of the year to calculate the statistical
196 significance of the MJO composites. Each iteration of the permutation test scrambles the years of
197 the MJO data while preserving day of the year. We perform 1000 permutations. The p-value of
198 the composite is $2 \times \min(f, 1 - f)$ where f is the fraction of permutations whose composites equal
199 or exceed the observed composite. The design of the permutation test accounts for the seasonality
200 and autocorrelation of the data.

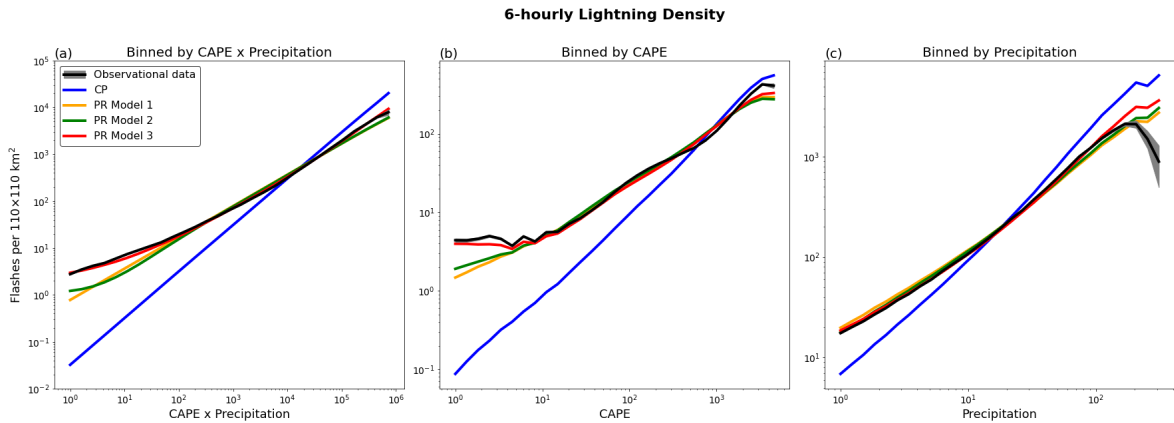
201 The Wilcoxon rank sum and permutation tests are performed at each grid point. The false
202 discovery rate (FDR) procedure from Benjamini and Hochberg (1995) is used to assess the statistical
203 significance of the correlation and (difference) composite maps. The two-sided p-value is calculated
204 at every land grid point and sorted from smallest to largest. Then, the sorted p-values are compared
205 to the sequence $\alpha/S, 2\alpha/S, 3\alpha/S, \dots$, where S is the number of land grid points ($S = 860$) and α is
206 the selected FDR, which we set at 10% here.

207 **3. Results**

208 *a. PR Model Development and Performance*

209 We begin by comparing the environmental dependence of the flash count data with that of CP
210 and the three PR models. First, we examine their dependence on $\text{CAPE} \times \text{Precipitation}$ (which is
211 proportional to CP), CAPE, and precipitation separately (Fig. 1). The flash density data binned by
212 $\text{CAPE} \times \text{Precipitation}$ show an approximate power-law dependence (linear on a log-log plot; Fig.
213 1a black line). The slope of the binned flash density data on the log-log plot is less than one which
214 differs substantially from that of CP (blue line) whose slope is equal to 1 by construction. The PR
215 Model 1 with slope equal to 0.726 (Table 1; Fig. 1a orange line) better matches the flash count
216 data. In the PR Model 2, the CAPE and precipitation exponents are fairly close to each other (0.684
217 and 0.754) to that of $\text{CAPE} \times \text{Precipitation}$ in the PR Model 1. The dependence of PR Model 2

218 on CAPE \times Precipitation (green line) is nearly indistinguishable from that of PR Model 1 (orange
 219 line). With the addition of squared log terms, the PR Model 3 is able to match the departure of the
 220 flash data from pure power-law dependence on CAPE \times Precipitation. Binning the observed flash
 221 data, CP, and the three PR models by CAPE and precipitation separately show similar behavior
 222 (Fig. 1b, c). The dependence of CP is mostly linear when binned by CAPE and precipitation
 223 separately but this behavior is not guaranteed by the functional form of CP. The mismatch between
 224 the dependence of CP and observed flash density on CAPE is larger than that for precipitation.



225 FIG. 1. Comparison of average 6-hourly lightning density (flashes per 110 \times 110 km² i.e., 1 $^\circ$ \times 1 $^\circ$ grid box at the
 226 equator) with the CP proxy and PR models binned by (a) CAPE \times Precipitation values, (b) CAPE values, and
 227 (c) Precipitation values. Observed data is shown with black line, with the gray shading indicating the expected
 228 range of 95% of the means. Values for the CP proxy and PR models are shown with the respective colored lines.
 229 See Table 1 for the variables and coefficients of the PR models tested.

TABLE 1. Summary of the Poisson regression models tested.

	PR Model 1		PR Model 2		PR Model 3	
Deviance	6.493 \times 10 ⁸		6.483 \times 10 ⁸		6.385 \times 10 ⁸	
Predictor	<i>Coef</i>	<i>95% Conf. Int.</i>	<i>Coef</i>	<i>95% Conf. Int.</i>	<i>Coef</i>	<i>95% Conf. Int.</i>
intercept	-0.911	[-0.930, -0.861]	-0.709	[-0.719, -0.680]	0.393	[0.380, 0.418]
log(CP)	0.726	[0.723, 0.730]	–	–	–	–
log(CAPE)	–	–	0.684	[0.683, 0.689]	0.250	[0.249, 0.260]
log(Precipitation)	–	–	0.754	[0.750, 0.760]	0.634	[0.631, 0.641]
log(CAPE) ²	–	–	–	–	0.0390	[0.0385, 0.0400]
log(Precipitation) ²	–	–	–	–	0.0327	[0.0323, 0.0335]

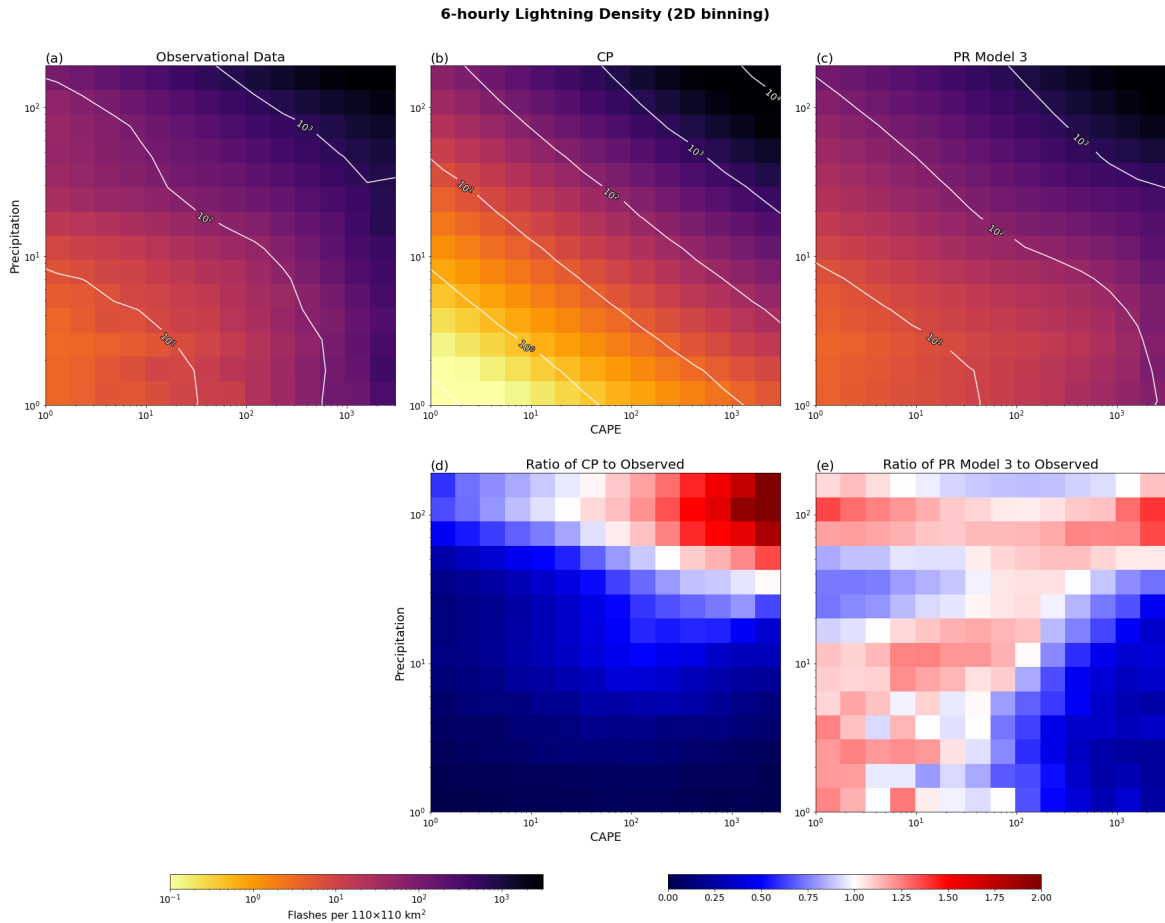
230 Figure 2 shows the joint dependence of the flash density, CP, and PR Model 3 on CAPE and
 231 precipitation. The isolines of the flash density data (Fig. 2a white lines) are not straight lines
 232 on the log-log axes, further indicating the departure of flash density data from pure power-law
 233 dependence on CAPE and precipitation, especially for low values of precipitation (i.e., CAPE
 234 matters more). On the other hand, the isolines of CP are linear. Consequently, CP underestimates
 235 flash density for low values of CAPE and precipitation and overestimates flash density for high
 236 values of CAPE and precipitation (Fig. 2b, d). The isolines of PR Model 3 better match the
 237 behavior of the observed isolines of the flash count data (Fig. 2c). Overall, the PR Model 3 better
 238 fits the observed dependence of flash counts on CAPE and precipitation than does the CP proxy,
 239 especially for extreme low or high values of CAPE and precipitation (Fig. 2e). The PR Model 3
 240 for 6-hourly lightning is:

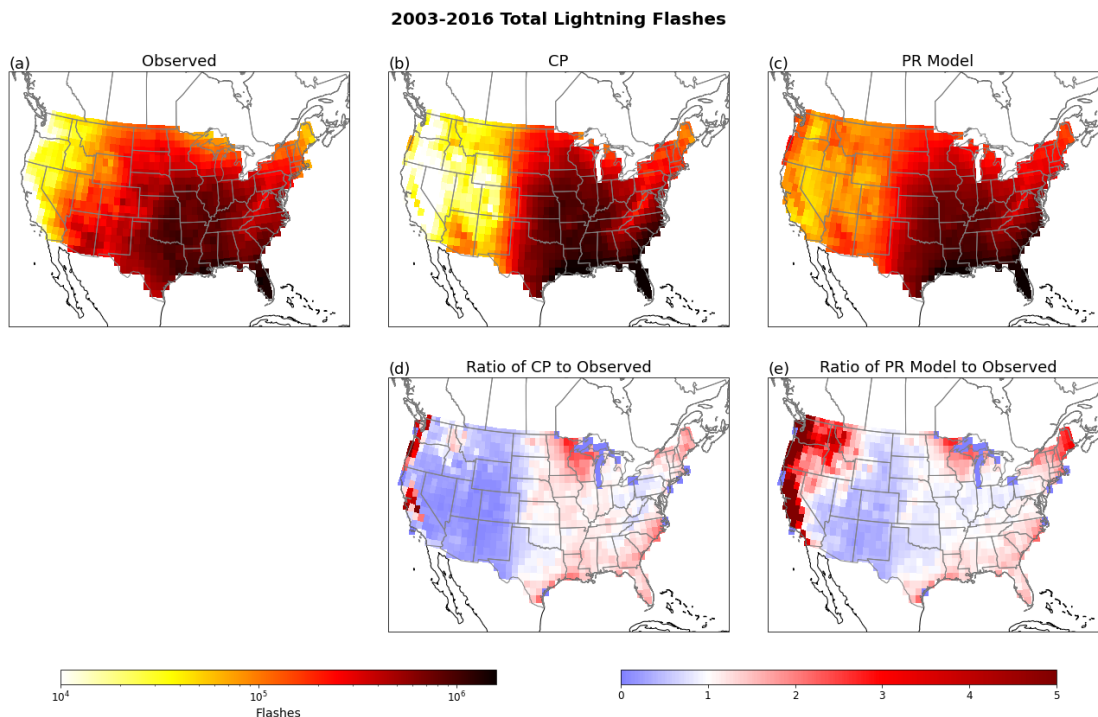
$$\begin{aligned}
 \mu = \exp[0.393 + 0.25 \log(\text{CAPE}) + 0.039(\log(\text{CAPE}))^2 + \\
 0.634 \log(\text{Precipitation}) + 0.0327(\log(\text{Precipitation}))^2] \Delta \text{lat} \Delta \text{lon} \cos \phi
 \end{aligned}
 \tag{4}$$

241 The remainder of the analysis, including all descriptions of PR predicted lightning, will use PR
 242 model 3.

250 Maps of the total lightning flashes for 2003–2016 show where lightning flashes occur most and
 251 least often. Observed lightning flash counts are highest along the Gulf Coast and Great Plains and
 252 are lowest along the West Coast (Fig. 3a). This overall pattern is reproduced by the CP proxy and
 253 PR model east of the Rocky Mountains (Fig. 3b,c). Both CP and the PR model underestimate
 254 flash counts over the Rocky Mountain states (west of 100°W) and overestimate flash counts over
 255 the West Coast and Upper Midwest (Fig. 3d,e). The largest bias in magnitude is over the West
 256 Coast, while the largest bias in spatial extent is over the Rocky Mountains. The bias of the PR
 257 model is reduced compared to that of CP (i.e., ratio closer to 1) over the Rocky Mountains and
 258 Upper Midwest (Fig. 3e). However, the PR overestimation of flash counts is increased over the
 259 West Coast and Pacific Northwest.

260 One possible reason that the PR model performs worse than the CP proxy on the West Coast and
 261 Pacific Northwest is that the PR model coefficient for $\log(\text{Precipitation})$ is greater than $\log(\text{CAPE})$
 262 (0.634 versus 0.25, respectively; cf. Table 1), whereas the CP proxy weights CAPE and precipitation
 263 equally. Climatologically, CAPE values are low across the western U.S., but the West Coast



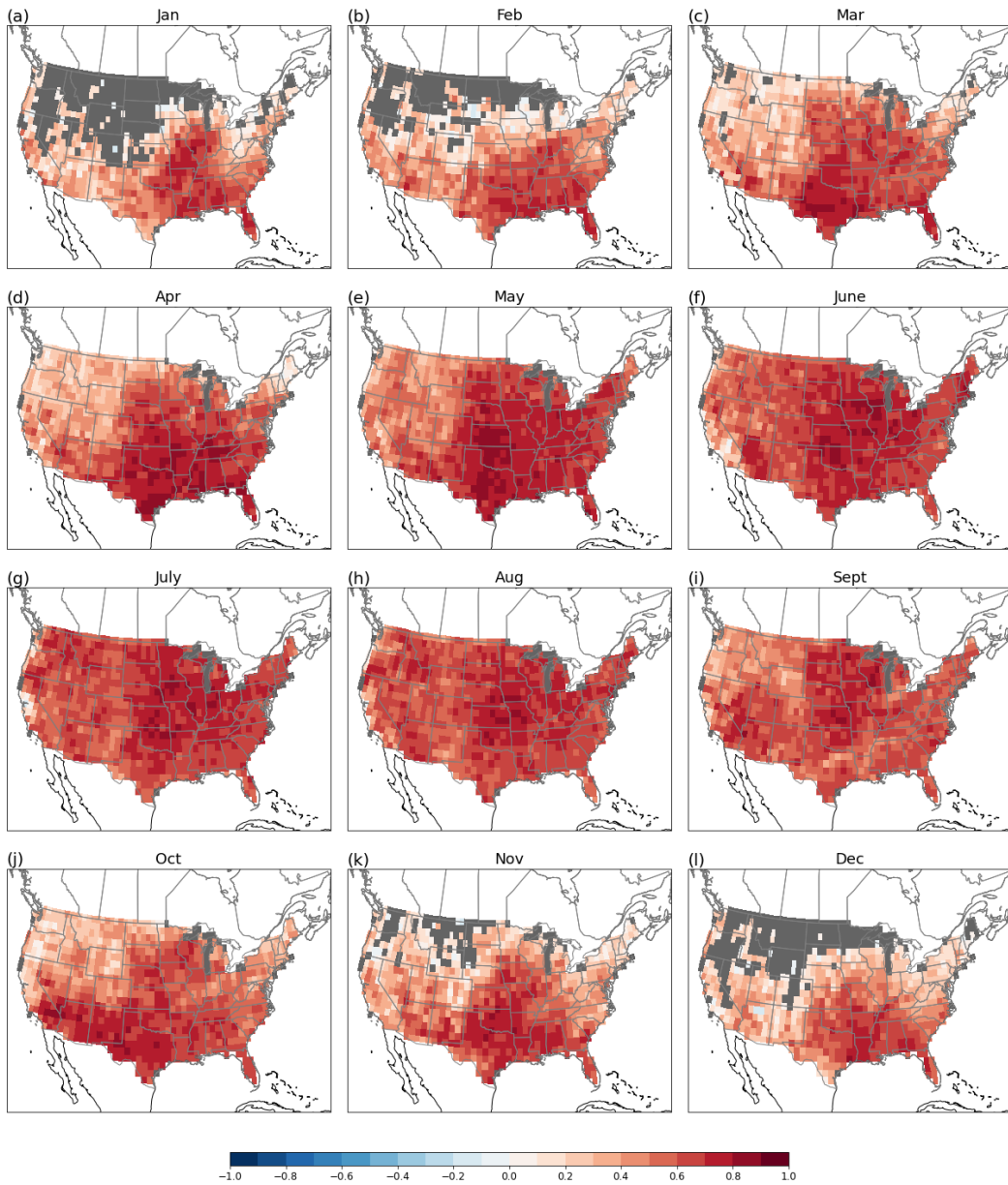


247 FIG. 3. (top) Number of lightning flashes between 2003–2016 in observations, using the CP proxy, and using
 248 the PR model. (bottom) Ratio between CP proxy total lightning flashes and observed total lightning flashes, and
 249 ratio between PR predicted total lightning flashes and observed total lightning flashes.

271 improved fit of the PR model to the observed data compared to the CP proxy, we drop the CP proxy
 272 and focus on the PR model.

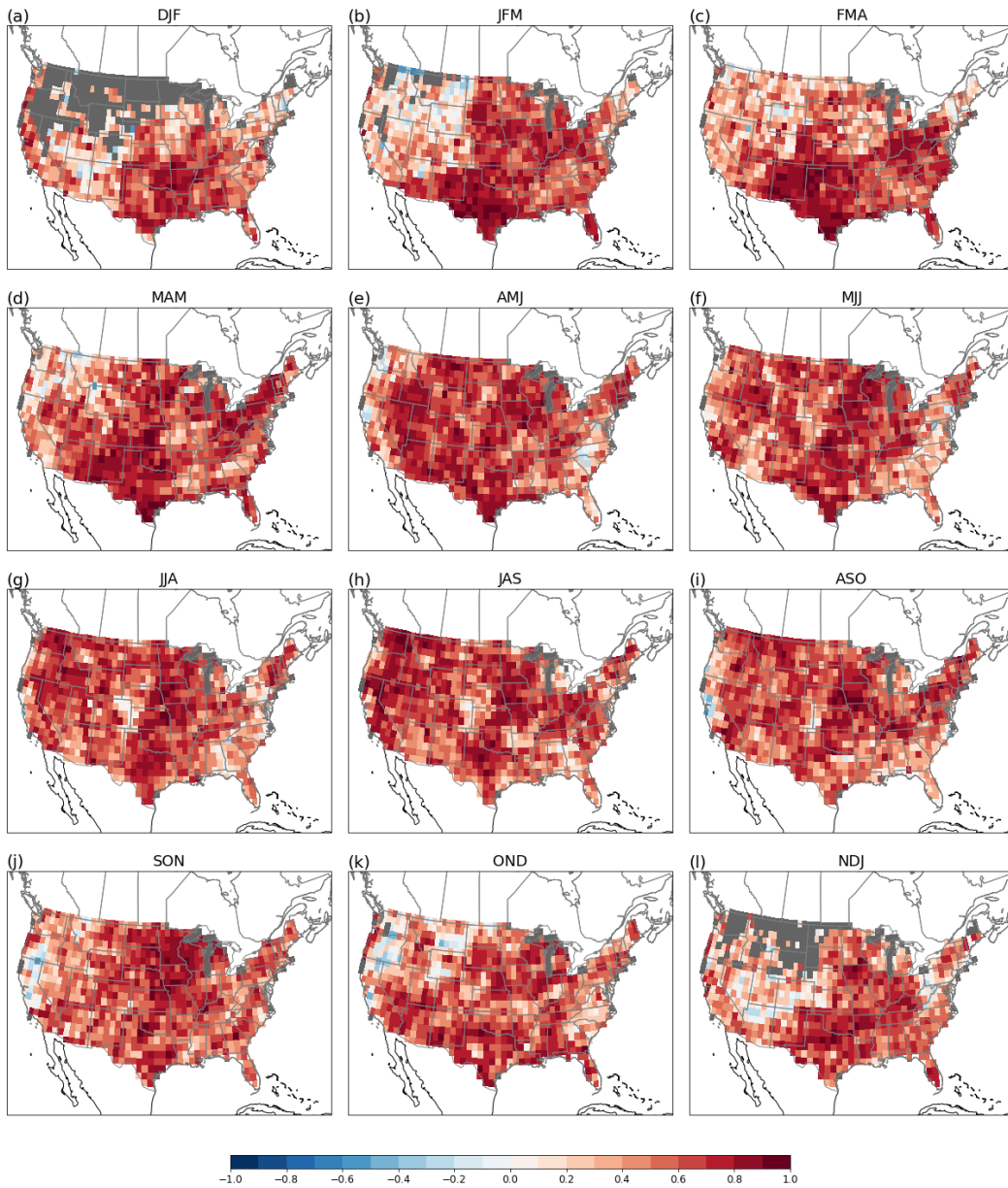
279 The degree to which the PR model matches observed variability varies depending on season
 280 and region. We focus on the rank correlation between observed and PR predicted flash counts
 281 at daily and seasonal time resolution because these are the relevant timescales for MJO and
 282 ENSO influences, respectively. PR model performance for daily data is greatest east of the Rocky
 283 Mountains during the warm season (April–September). Skill is worse over the Northwest U.S.,
 284 Northern Plains, and Northeast U.S. during the cool season (October–March; Fig. 4a-c, k, l). These
 285 regions of low skill are located where, climatologically, there are few lightning flashes (but more
 286 than 10 lightning flashes occurred during the 14-year period in that month and so were not masked)
 287 and low variance in lightning (cf. Fig. 3; Tippett et al. 2019). PR model performance for seasonal
 288 totals (Fig. 5) is similar to that for daily data, but spatially the correlation skill is noisier due to

2003-2016 Rank Correlation between Daily Observed and PR Predicted Data by Month



273 FIG. 4. 2003–2016 Grid point rank correlation between daily observed and PR predicted flash anomalies
274 grouped by month. Sample size is the number of days in month times 14 years. Gray grid points indicate where
275 10 or fewer observed lightning flashes occurred over the 14-year period for that particular month.

2003–2016 Rank Correlation between Seasonal Observed and PR Predicted Data



276 FIG. 5. 2003–2016 Grid point rank correlation between seasonal observed and PR predicted flash anomalies.
277 Sample size is 14 years. Gray grid points indicate where 30 or fewer observed lightning flashes occurred over
278 the 14-year period for that particular season.

289 the smaller sample size. Interestingly, despite the high rank correlation in daily summer flashes
290 over the Southeast U.S., rank correlation for the summer seasonal totals for the Southeast U.S. is
291 reduced. Overall, skill is low over the West Coast, Northwest U.S., and eastern U.S., especially
292 during the winter (cf. Fig. 5a, b, k, l).

293 Seasonal and regional details of PR model skill are summarized in Tables 2 and 3. Some of
294 these temporal rank correlation values are higher than would be expected from the spatial rank
295 correlation maps for winter (cf. Fig. 4l vs. Table 2 Dec in top row) and are lower than would
296 be expected from the spatial rank correlation maps for summer (cf. Fig. 4g vs. Table 2 July in
297 top row), demonstrating that spatial aggregation can increase or decrease correlation. There is
298 a statistically significant correlation between daily observed and PR predicted total lightning
299 flash counts east of 120°W (CONUS excluding the West Coast) year-round (Table 2 top row).
300 Daily PR predicted total flashes are highly correlated with daily observed total flashes during
301 winter and spring in particular. There is a statistically significant correlation between seasonal
302 observed and PR predicted total lightning flash counts east of 120°W during October through
303 June, excluding the MAM season (Table 3 top row). In the warm season, correlations between
304 daily observed and PR predicted total flashes are higher than correlations between seasonal
305 observed and PR predicted total flashes (top rows of Table 2 Apr through Oct vs. Table 3 MAM
306 through SON). During the warm season, when there are high day-to-day values and fluctuations
307 in flash counts, temporal aggregation (via a seasonal summation) does not improve PR model
308 performance. Conversely, in DJF and JFM, correlations between seasonal observed and PR
309 predicted total flashes are higher than correlations between daily observed and PR predicted total
310 flashes (top rows of Table 2 Jan and Feb vs. Table 3 DJF and JFM). Unlike during the warm
311 season, temporal and spatial aggregation of flashes during the cool season benefits correlation skill.

312
317 Although the model fails to capture CONUS-wide seasonal flash count during some parts of
318 the year, it still performs well for some regions after spatial aggregation. For example, seasonal
319 PR predicted total CONUS flash counts in summer and fall are poorly correlated with observed
320 total CONUS flash counts (Table 3 top row), but predicted total flash counts are well correlated
321 with observed total flash counts over the Northwest and Southwest (Table 3 second and third row).
322 Despite some large regional biases in lightning climatology, the variability is well captured by

313 TABLE 2. Rank correlations between observed and PR predicted daily total flashes within region, grouped by
 314 month. All (bolded) correlations are considered significant at the 1% level.

	Jan	Feb	Mar	Apr	May	June	July	Aug	Sept	Oct	Nov	Dec
CONUS East of 120°W	0.8	0.88	0.88	0.89	0.85	0.72	0.66	0.67	0.67	0.70	0.77	0.86
Northwest [41-50°N, 102-125°W]	0.59	0.63	0.69	0.60	0.77	0.80	0.86	0.85	0.72	0.60	0.69	0.69
Southwest [30-41°N, 102-125°W]	0.70	0.78	0.71	0.78	0.85	0.82	0.66	0.66	0.80	0.86	0.78	0.72
Tennessee River Valley [33-42°N, 84-93°W]	0.71	0.73	0.82	0.92	0.89	0.84	0.85	0.86	0.81	0.80	0.79	0.77
Northeast [37-50°N, 65-90°W]	0.63	0.57	0.72	0.84	0.86	0.86	0.88	0.85	0.80	0.70	0.61	0.64
Southeast [24-37°N, 76-85°W]	0.74	0.82	0.87	0.91	0.88	0.64	0.68	0.66	0.75	0.85	0.78	0.79

315 TABLE 3. Rank correlations between observed and PR predicted seasonal total flashes within region. Bolded
 316 correlations are considered significant at the 10% level.

	DJF	JFM	FMA	MAM	AMJ	MJJ	JJA	JAS	ASO	SON	OND	NDJ
CONUS East of 120°W	0.91	0.95	0.82	0.32	0.51	0.64	0.41	0.4	0.33	0.35	0.76	0.81
Northwest [41-50°N, 102-125°W]	0.61	0.0	0.03	0.0	0.42	0.48	0.64	0.82	0.71	0.74	0.31	0.77
Southwest [30-41°N, 102-125°W]	0.54	0.68	0.87	0.84	0.94	0.5	0.63	0.51	0.56	0.54	0.89	0.38
Tennessee River Valley [33-42°N, 84-93°W]	0.85	0.92	0.64	0.44	0.58	0.77	0.58	0.27	0.31	0.44	0.52	0.75
Northeast [37-50°N, 65-90°W]	0.62	0.82	0.81	0.60	0.42	0.13	0.04	0.16	0.30	0.67	0.70	0.64
Southeast [24-37°N, 76-85°W]	0.59	0.78	0.63	0.46	0.09	0.12	0.19	0.35	0.07	0.32	0.66	0.73

323 the model. This is especially true when using rank correlation, which is insensitive to systematic
 324 amplitude errors.

325 In brief, we determined that the PR model can generally reproduce many of the observed aspects
 326 of the climatology and variability of lightning. The MJO analysis during JJAS with daily data in
 327 the next subsection is appropriate given the PR model performance is good over these months and
 328 over all regions on this timescale. Similarly, ENSO analysis during DJF through MJJ is generally
 329 appropriate given PR model performance during these seasons. There are noted discrepancies,
 330 e.g., poor performance over Northwest during winter through midspring, that should be kept in
 331 mind.

332 *b. MJO-Lightning Relationship*

333 Motivated by previous work that found statistically significant relations between active MJO
 334 phases and CONUS lightning activity during JJAS (Abatzoglou and Brown 2009), we computed

335 maps of anomalous flash counts during active MJO phases for the period 2003–2016 (Supple-
336 mentary Fig. S1). We found essentially no statistically significant flash count anomalies in any of
337 the MJO phases. Although the period is relatively short, the number of active phase days in the
338 analysis is not excessively small; phase 7 has the fewest active days (63), and phase 1 has the most
339 (237). We conclude that any MJO signal in flash counts is too modest to be robustly detected in
340 this sample.

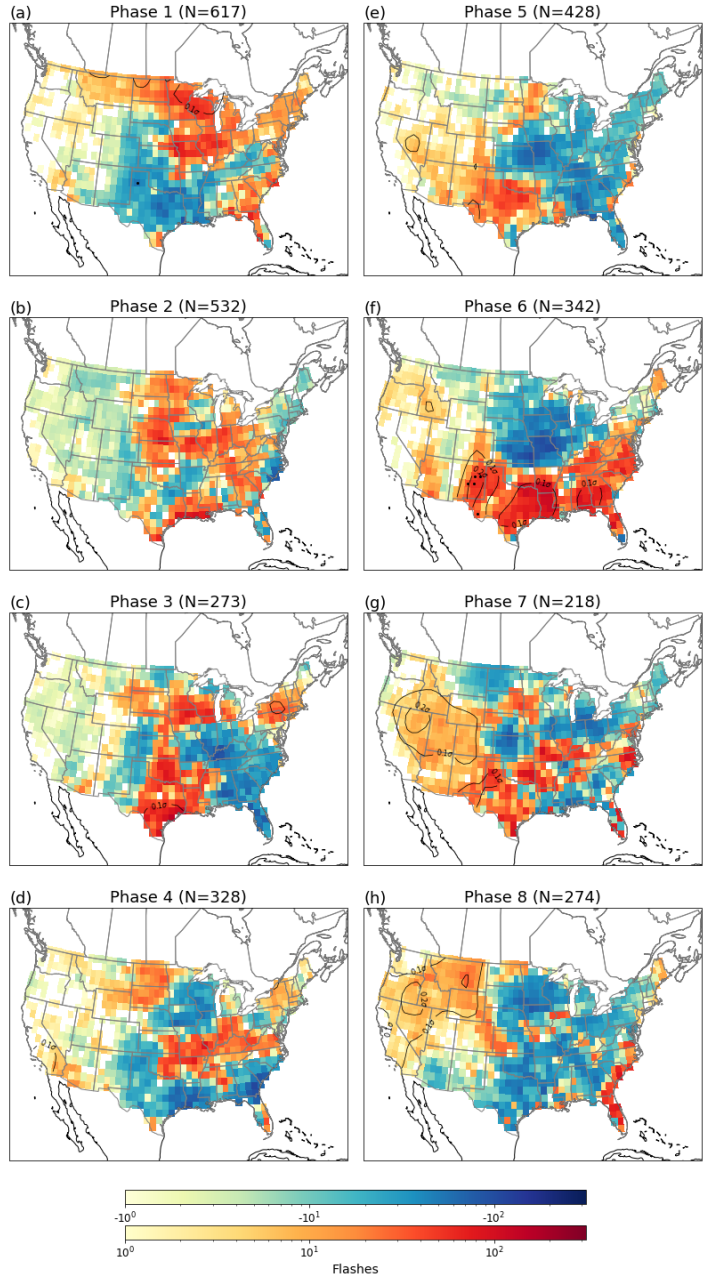
341 We repeated the MJO composite analysis using the PR predicted values over the same 2003–2016
342 period and again found essentially no statistically significant anomalies in any of the MJO phases
343 (Supplementary Fig. S2). Nevertheless, PR predicted flash anomaly composites show that the PR
344 model is at least broadly capturing similar patterns to the observations on the days that go into the
345 MJO composites. The average (over MJO phases) pattern correlation between the observed and
346 PR predicted flash anomaly composites is 0.65.

347 The relatively good relation between flash count and PR composites in addition to the strong
348 rank correlation of PR with daily flash counts during this time of year (Fig. 4) substantiates the
349 strategy of using the PR model to examine the MJO-lightning relationship in the longer period
350 1979–2021 during which reanalysis data are available. Using a long period permits the detection
351 of MJO signals that were too small to be detected in the 14-year lightning data set.

352 Despite the longer period, we also find for the 1979–2021 period that there are essentially no
353 statistically significant PR flash anomalies in any of the MJO phases (Fig. 6), and anomalies are
354 relatively small (at most, 0.1-0.2 standard deviations away from climatology in some regions).
355 While some of the 1979–2021 PR predicted patterns are consistent with the 2003–2016 observed
356 patterns (e.g., MJO phase 6 composites), the lack of statistical significance from the permutation test
357 and FDR correction suggests these similarities might be due to chance rather than MJO variability.

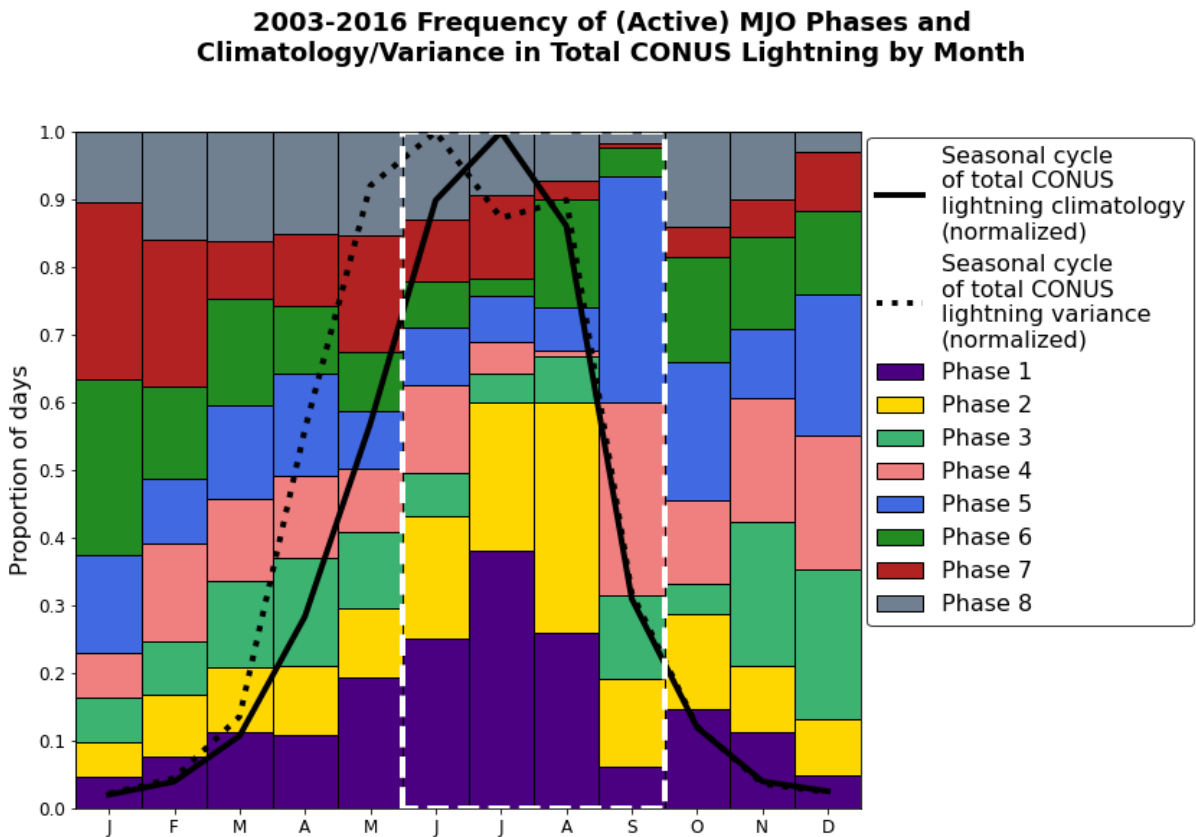
361 These MJO-lightning results differ from Abatzoglou and Brown (2009), which found statistically
362 significant relations between MJO phase and JJAS lightning counts. Like the study here, they
363 used NLDN data at daily resolution aggregated to a $1^\circ \times 1^\circ$ grid. Some data and methodological
364 differences might explain the differing results. For example, Abatzoglou and Brown (2009) used
365 JJAS lightning data for the period 1990–2007 which differs from the 2003–2016 period used here.
366 However, our PR modeled data analysis over longer period 1979–2021 also found no statistically
367 significant associations. In addition, they assessed statistical significance using a Wilcoxon rank

**1979-2021 JJAS Composite
Predicted Daily Lightning Flash Anomaly by MJO Phase**



358 FIG. 6. 1979–2021 JJAS composites of PR predicted flash count anomalies by (active) MJO phase. Anomalies
 359 are with respect to a daily climatology. Black contours indicate anomalies that are 0.1 and 0.2 standard deviations
 360 away from climatology. Black stippling indicates statistically significant values.

368 sum test and did not account for multiple testing. We used a permutation test and a FDR control
 369 procedure. Accounting for multiple testing is important because when a statistical significance test
 370 is applied at many grid points with, for instance, $\alpha = 0.05$, then the null hypothesis is expected to
 371 be rejected 5% of the time when it is true (type I error), and the presence of spatial correlation
 372 leads to an even higher type I error rate (Wilks 2016). The FDR procedure used here is designed
 373 to avoid such type I errors. Moreover, its behavior here appears to be reasonable (i.e., not overly
 374 strict) since before the FDR procedure, on average, only 8% of the land points pass the statistical
 375 significance test at the nominal 5% level.



376 FIG. 7. 2003–2016 Proportion of days in each (active) MJO phase, with overlaid seasonal cycle of total CONUS
 377 lightning climatology (solid black) and variance (dotted black). White dashed box denotes season of interest for
 378 MJO-lightning analysis.

379 Of the possible explanations for the differing results, the application of the Wilcoxon rank sum
380 test deserves attention. The Wilcoxon rank sum test addresses the question of whether two sets of
381 samples come from the same distribution. In particular, the Wilcoxon rank sum test is designed
382 to detect *stochastic dominance*. A random variable X has stochastic dominance over a random
383 variable Y if $P(X > z) \geq P(Y > z)$ for all thresholds z and is strictly greater for some thresholds.
384 In the application here, the Wilcoxon rank sum test decides whether the observed lightning flash
385 counts are higher for a particular MJO phase compared to the other phases. This comparison
386 assumes that all other factors are held fixed, and, when that is not the case, a confounding factor
387 can produce an apparent relation in variables that are otherwise unrelated (DelSole and Tippet
388 2022). The annual cycle is the most common confounding factor in climate studies, and not
389 accounting for it leads to detecting links in quantities whose only link is that they share annual
390 cycle phasing. Fig. 7 shows that CONUS lightning count mean (solid black line) and variance
391 (dashed black line) have strong seasonality, with highest values in summer. MJO phase frequency
392 also presents seasonality (Fig. 7 color bars), especially in the 14-year period considered here. It
393 is possible, for example, that the mostly negative JJAS flash anomalies in MJO phase 5 (Fig. 6e)
394 might be due to phase 5 being most frequent in September when lightning activity is relatively
395 low. We assessed the impact of failing to account for seasonality by applying the Wilcoxon rank
396 sum test to data whose seasonality exactly matched that of the observed flash count data but which
397 had no relation with MJO phase. We constructed such a dataset by randomly permuting the years
398 of the summed CONUS lightning flash count data while maintaining day of the year. We then
399 applied the Wilcoxon rank sum test with a significance level of $\alpha = 0.05$. In this situation the null
400 hypothesis of no relation is true, and p-values < 0.05 constitute type I errors. We computed type
401 I error rates for each MJO phase and repeated this procedure with 1000 random permutations of
402 the years. Table 4 (first row) shows the type I error rates are far from their desired value of 5%.
403 We note that removing the seasonal mean leaves the ranks unchanged and likewise the results of
404 the rank sum test are the same. One strategy to account for seasonality is to remove the daily flash
405 count climatology. Table 4 (second row) shows that removing the daily flash count climatology
406 reduces the type I error rates but they remain far from their desired value of 5%. Seasonality of
407 the lightning flash count variance as well as autocorrelation are possible reasons why removal of
408 the daily climatology was inadequate. On the other hand, the permutation test which accounts

409 for seasonality and autocorrelation has type I error rates that are close to 5% (Table 4 third row).
 410 Hence, we conclude that the difference between previous results and ours regarding MJO-lightning
 411 links may be due at least in part to differences in statistical significance testing methodology.

412 TABLE 4. Type I Error Rate at the 0.05 significance level, which is $\text{Freq}(p\text{-value} < 0.05)$, using the Wilcoxon
 413 rank sum test for the observed 2003–2016 MJO composites and randomized lightning flash data (top row) with
 414 seasonal mean removed, (middle row) with daily mean removed, and (bottom row) using the permutation test.

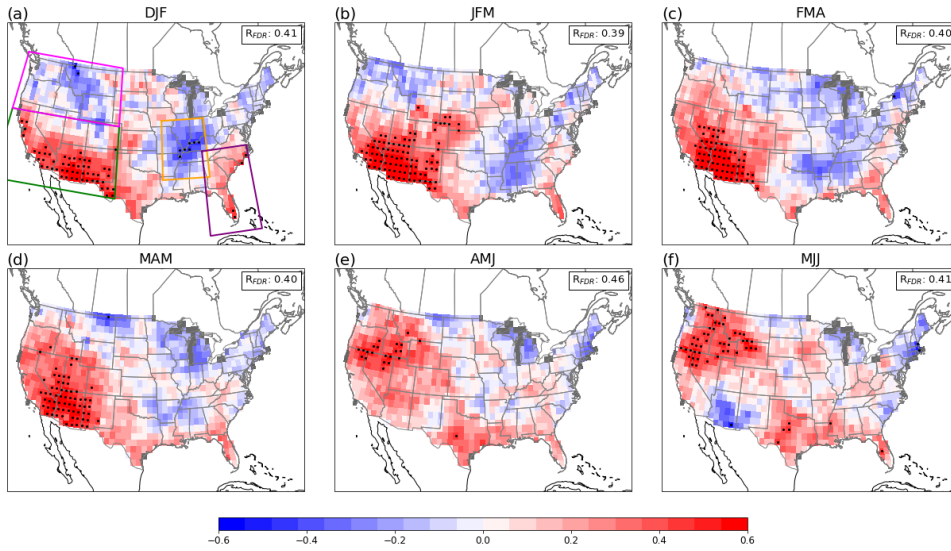
Phase	1	2	3	4	5	6	7	8
Rank sum test, removed seasonal climatology	0.98	0.34	0.82	0.99	1.0	0.21	0.69	0.59
Rank sum test, removed daily climatology	0.18	0.24	0.20	0.16	0.10	0.25	0.26	0.26
Permutation test	0.05	0.05	0.04	0.04	0.06	0.04	0.06	0.05

415 *c. ENSO-Lightning Relationship*

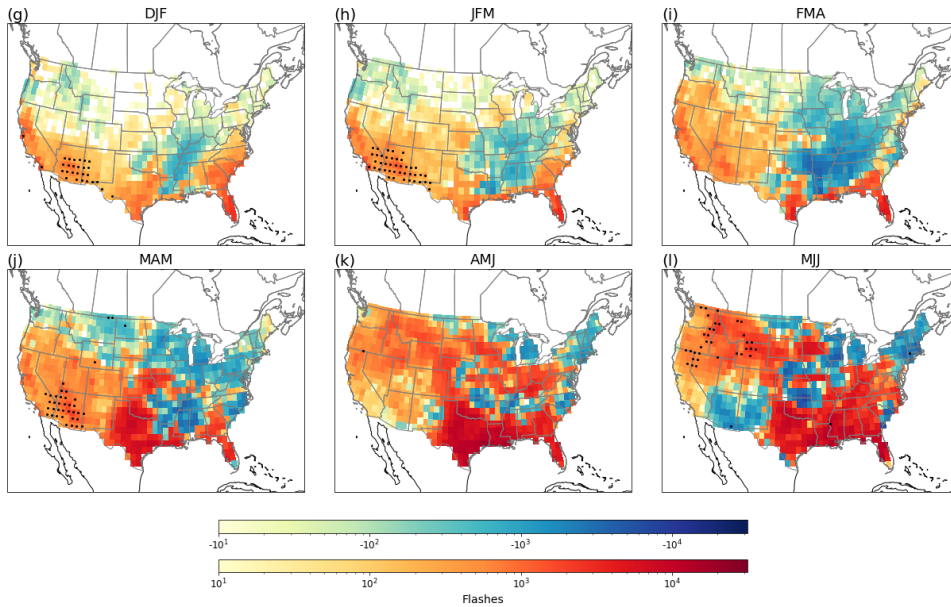
416 We first examined ENSO influence on observed and PR predicted lightning activity for the 2003–
 417 2016 period during the six 3-month overlapping seasons DJF–MJJ. Because the period is short and
 418 contains few ENSO events (4 complete El Niño events and 5 complete La Niña events), statistical
 419 significance is not expected. Maps of rank correlation between ONI and observed lightning
 420 flash anomaly (Supplementary Figs. S3a–f) and maps of El Niño - La Niña difference composites
 421 (Supplementary Figs. S3g–l) show no statistical significance. Likewise, the PR predicted data show
 422 no statistically significant evidence for an ENSO signal during the period 2003–2016 in either rank
 423 correlations or difference composites (Supplementary Figs. S4a–f and S4g–l, respectively). Rank
 424 correlations between ONI and regionally summed lightning flash count anomalies for DJF–MJJ
 425 (Fig. S5) show: mostly positive correlations for the Northwest and statistical significance for FMA–
 426 MJJ, positive correlations for the Southwest and and statistical significance for DJF–MJJ, negative
 427 correlations for the Tennessee River Valley and statistical significance in FMA, and mostly negative
 428 values for the Coastal Southeast but no statistical significance.

429 The similarities between the observed and PR results for ENSO rank correlations (average pattern
 430 correlation 0.59) and for ENSO composites (average pattern correlation 0.64) further supports using
 431 the PR model to examine the ENSO-lightning relation in the longer period 1979–2021. In addition,
 432 rank correlations between ONI and the regionally summed lightning flash anomalies are generally
 433 consistent for all regions.

1979-2021 Rank Correlation between PR Predicted Seasonal Lightning Flash Anomaly and ENSO

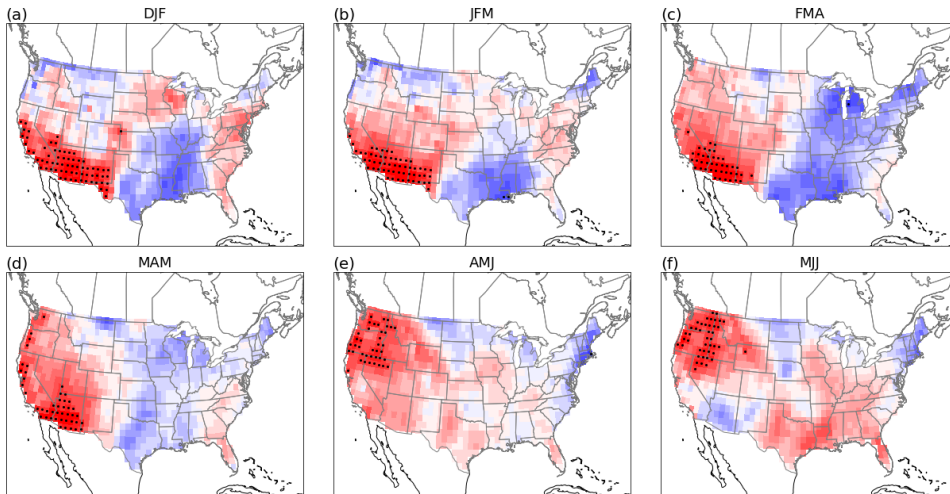


1979-2021 El Niño - La Niña Difference Composite of Predicted Seasonal Lightning Flash

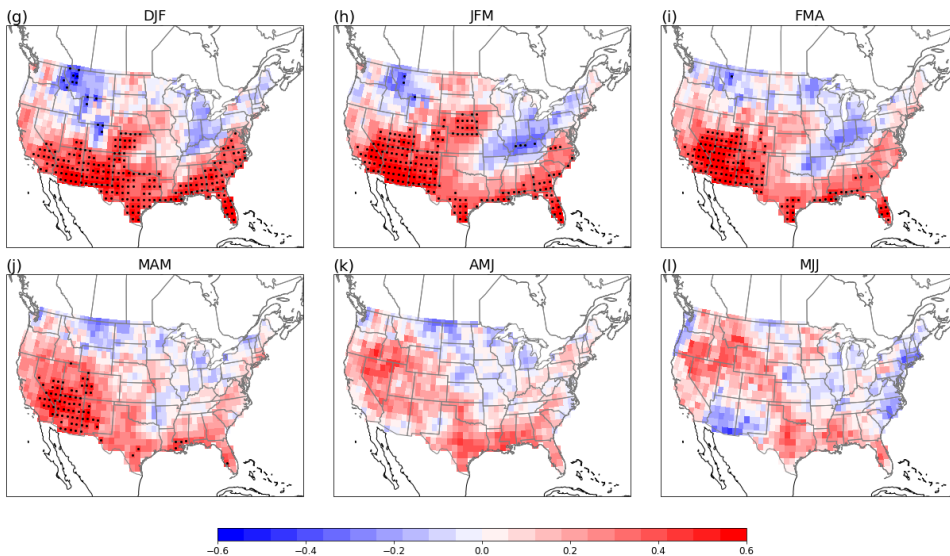


434 FIG. 8. (a-f) 1979–2021 Rank correlation between PR predicted seasonal lightning flash count anomalies and
 435 ONI. All insignificant correlations have amplitudes less than R_{FDR} , which is shown in top-right panel. (g–l)
 436 1979–2021 difference composites (El Niño - La Niña) of PR predicted seasonal lightning flash count anomalies.
 437 Black stippling indicates statistically significant values. Domain boxes in panel (a) indicate regions of interest
 438 (see text for details).

1979-2021 Rank Correlation between Seasonal CAPE Anomaly and ENSO



1979-2021 Rank Correlation between Seasonal Precipitation Anomaly and ENSO



439 FIG. 9. 1979–2021 Rank correlation between ONI and (a–f) seasonal CAPE anomaly and (g–l) seasonal
 440 precipitation anomaly. Black stippling indicates statistically significant values.

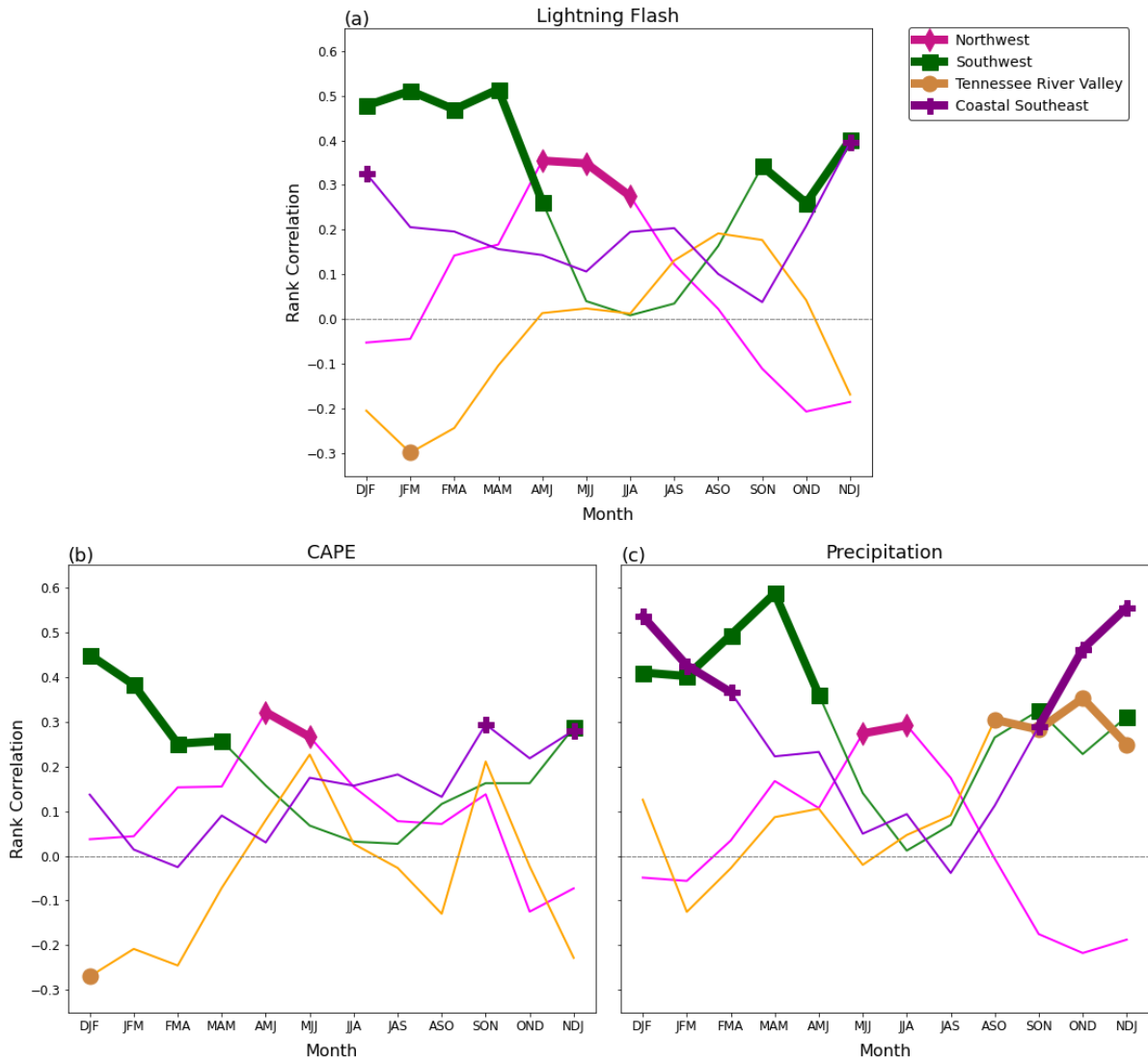
441 We use rank correlation maps (Figs. 8a–f) and El Niño - La Niña difference composites (Fig.
 442 8g–l) to examine the relation between ENSO and PR predicted lightning activity during winter
 443 and spring over the longer period 1979–2021. The two measures are complementary, with rank
 444 correlation showing the strength of the relationship and the El Niño - La Niña difference composites

445 showing their expected magnitude. Four regions stand out as having large-scale ENSO signals
446 during some periods in winter and spring: Northwest, Southwest, Tennessee River Valley, and
447 Coastal Southeast. The domains for these regions are displayed in Fig. 8a and described in Tables 2
448 and 3. The rank correlation maps indicate more regions with statistically significant links between
449 ENSO and PR predicted lightning, likely because correlation utilizes the full dataset, as well
450 as ONI amplitude, and is less sensitive to outliers than the composites. During the midwinter
451 months, El Niño has a modest relationship with increased PR lightning activity over the Coastal
452 Southeast (Fig. 8a), with expected ENSO-modulated PR lightning activity on the order of 10^2
453 to 10^3 flashes (~ 30 - 40% more than normal; Fig. 8g). During the winter through early spring
454 months, El Niño is associated with increased PR lightning activity over the Southwest, and La
455 Niña is associated with increased PR lightning activity over the Tennessee River Valley (Fig. 8a,
456 b), though the signal over the Tennessee River Valley is statistically significant only for the DJF
457 season. Because this season has fewer flashes climatologically (Tippett et al. 2019), the expected
458 difference in ENSO-modulated PR lightning activity is on the order of 10^2 flashes ($\sim 30\%$ more
459 than normal; Fig. 8g, h), though locally differences are on the order of 10^3 flashes. During spring,
460 El Niño is associated with increased PR lightning activity over the Southwest (Fig. 8c, d), and
461 the difference in ENSO-modulated PR lightning activity is on the order of 10^2 in FMA (~ 40 - 50%
462 more than normal; Fig. 8i) and 10^3 flashes in MAM (~ 50 - 60% more than normal; Fig. 8j). El
463 Niño is associated increased PR lightning activity over the Northwest in the late spring (Fig. 8e,
464 f). However, the difference composites do not indicate a clear positive signal related to El Niño
465 (Fig. 8k, l), suggesting there might be asymmetries between the El Niño- and La Niña-modulated
466 patterns of PR lightning activity in this region.

467 We explain ENSO influence on PR predicted lightning activity in these regions and seasons
468 by examining the relationship between ENSO and the large-scale environmental variables in the
469 PR model, CAPE and precipitation. The ENSO-precipitation relationship helps explain ENSO
470 modulation during winter over the Coastal Southeast during midwinter (cf. Fig. 9g vs. Fig. 8a).
471 The ENSO-CAPE relationship helps best explains ENSO modulation of lightning activity over
472 the Tennessee River Valley, including its peak in winter through early spring (cf. Fig. 9a-c vs.
473 Fig. 8a-c). Both CAPE and precipitation can be useful explanatory variables to describe ENSO

474 modulation patterns and seasonality over the Southwest (cf. Figs. 9a-d and 9g-j vs. Fig. 8a-d) and
 475 Northwest (cf. Figs. 9e, f and 9k, l vs. Fig. 8e, f).

Rank Correlation between Regionally Averaged Anomaly and ENSO by Month



476 FIG. 10. 1979–2021 Rank correlation between ONI and regionally summed (a) PR predicted lightning flash
 477 anomaly, (b) CAPE anomaly, and (c) precipitation anomaly. Markers and any thicker lines between points
 478 indicate seasons when rank correlation is statistically significant at the 90% confidence level determined by
 479 bootstrapping method with 1000 iterations.

480 As a summary, we took each 3-month season of (PR predicted) regionally summed lightning
481 flash, CAPE, or precipitation anomaly for the Northwest, Southwest, Tennessee River Valley, or
482 Coastal Southeast and correlated it with ENSO (Fig. 10), which describes the major takeaways for
483 the 1979–2021 ENSO-lightning analysis:

- 484 • Over the Northwest, there is a positive correlation between ENSO and lightning activity -
485 hence El Niño (La Niña) is associated with increased (decreased) lightning activity - that peaks
486 in late spring and early summer (Fig. 10a magenta line). This is explained by El Niño-related
487 (La Niña-related) increases (decreases) in both CAPE and precipitation over the region (Fig.
488 10b, c magenta lines).

- 489 • Over the Southwest, there is a positive correlation between ENSO and lightning activity -
490 hence El Niño (La Niña) is associated with increased (decreased) lightning activity - that
491 peaks in the winter and spring (Fig. 10a green line). This is best explained by El Niño-related
492 (La Niña-related) increases (decreases) in both CAPE and precipitation over the region (Fig.
493 10b, c green lines).

- 494 • Over the Tennessee River Valley, there is a negative correlation between ENSO and lightning
495 activity - hence La Niña (El Niño) is associated with increased (decreased) lightning activity
496 - that peaks during winter (Fig. 10a gold line). This is best explained by La Niña-related (El
497 Niño-related) increases (decreases) in CAPE over the region (Fig. 10b gold line).

- 498 • Over the Coastal Southeast, there is a positive correlation between ENSO and lightning
499 activity - hence El Niño (La Niña) is associated with increased (decreased) lightning activity
500 - that peaks in winter (Fig. 10a purple line). This is best explained by El Niño-related (La
501 Niña-related) increases (decreases) in precipitation over the region (Fig. 10c purple line).

502 The weak ENSO signal in PR lightning activity over the Tennessee River Valley and Coastal
503 Southeast can perhaps be attributed to the contrasting ENSO signals in CAPE and precipitation.
504 For instance, when the ENSO-PR lightning link over the Tennessee River Valley is highest in late
505 winter, the ENSO-CAPE correlation is negative and the ENSO-precipitation correlation is positive
506 over the region.

507 **4. Summary and Discussion**

508 Despite its substantial impacts, relatively little is known about the relation of lightning with
509 predictable large-scale climate variability. In this study, we modeled 2003–2016 lightning activity
510 over the U.S. using Poisson regression (PR), relating lightning flash counts data to CAPE and
511 precipitation values. The PR model more accurately captured the dependence of flash counts on
512 the environmental factors compared to previous models. In particular, the PR model with the
513 best performance used $\log(\text{CAPE})$, $\log(\text{CAPE})^2$, $\log(\text{Precipitation})$, and $\log(\text{Precipitation})^2$ terms
514 as predictors. Correlations between the observed and PR predicted lightning flash counts at daily
515 and seasonal scales show that the PR model overall represents daily and seasonal variability well.
516 We did not detect a robust MJO-lightning or ENSO-lightning relationship for the short 2003–
517 2016 period, but we found observed and PR predicted patterns were similar. Therefore, with the
518 PR model, we constructed a lightning proxy for longer period 1979–2021. For the 1979–2021
519 period, we found no evidence that the lightning activity is related to active MJO phases during
520 JJAS. However, ENSO was associated with anomalous PR lightning flash patterns. La Niña is
521 associated with increased lightning activity over the Tennessee River Valley during winter, and El
522 Niño is associated with increased lightning activity over the Coastal Southeast during winter, the
523 Southwest during winter and spring, and the Northwest during late spring and early summer. In
524 terms of the magnitude of lightning flash anomalies during ENSO phases, most differences are
525 on the order of 10^2 more (or fewer) flashes per season except for some localized differences on
526 the order of 10^3 more flashes, e.g., Montana and Wyoming in early summer. The PR lightning
527 proxy also provides insight into how ENSO influences CAPE and precipitation patterns, including
528 the seasonal evolution of the ENSO-CAPE and ENSO-precipitation link. As a result, ENSO
529 may be a potentially useful predictor for winter through late spring lightning activity, valuable for
530 protecting public safety as well as for understanding increased risk of lightning-caused wildfires
531 and thunderstorm-related impacts.

532 The PR approach has its limitations. For example, western U.S, especially West Coast, lightning
533 climatology was not well represented. It has been found that lightning along the West Coast
534 involves different mechanisms/processes than lightning over the rest of the contiguous U.S. (Zipser
535 1994; Holle et al. 2016). The West Coast has a high number of positive CG flashes that are not
536 associated with severe weather (Zajac and Rutledge 2001; Koshak et al. 2015; Medici et al. 2017)

537 but might be associated with greater ice clouds (Fuchs et al. 2015; Mülmenstädt et al. 2015). The PR
538 model does not take into account other important environmental factors, e.g., wet-bulb temperature
539 (Koshak et al. 2015), warm cloud depth (Stolz et al. 2017), mid-level humidity (Westermayer et al.
540 2017), cloud top height (Finney et al. 2018), etc., which may limit its representation of lightning
541 across many climates and terrains. Noting the western U.S. deficiencies, fitting the data separately
542 shows a systematically different base rate and dependence on CAPE and precipitation that might
543 be due to differing precipitation/lightning processes or missing physics. We did find that we could
544 improve lightning climatology and skill by adding lifted condensation level (LCL) as a predictor
545 in the PR model (not shown), reducing the biases over the western U.S. by accounting for the
546 lower cloud bases, warm rain processes, and/or greater precipitation efficiency in the western U.S.
547 (Mülmenstädt et al. 2015; Fuchs et al. 2015; Tippett et al. 2019). Regardless, the PR model
548 with the LCL predictor did not impact nor improve representation of lightning variability and, by
549 extension, the MJO- or ENSO-lightning relationship, motivating the choice to exclude the LCL in
550 the model for the purpose of this study. While PR predicted lightning flash counts of the PR model
551 during 2003–2016 were comparable to observations, it is not guaranteed that the PR model would
552 perform well outside this data-fitting period, especially if there were long-term trends involved
553 (Stainforth et al. 2007; Camargo et al. 2014). Overall, MJO-lightning and ENSO-lightning results
554 were qualitatively similar when using the CP proxy predicted lightning data (not shown).

555 Because of the high variability of lightning and its strong seasonality, the PR model performs
556 better at daily resolution in the warm season and at seasonal resolution in the cool season (cf. Tables
557 2 and 3). During seasons and in regions with high lightning variability, temporal and/or spatial
558 aggregation does not improve PR model performance. This dependence of skill on timescale may
559 reflect that during climatologically active times of the year, aggregation over a season requires
560 accurate representation over many days, whereas during climatologically inactive times of the year,
561 aggregation over a season requires accurate representation over fewer days. Likewise, the depen-
562 dence of skill on region may reflect that over climatologically active locations, spatial aggregation
563 requires accurate representation over many grid points. The timescale of climate drivers as well as
564 season or region of interest should be considered when using the lightning proxy. For example, the
565 lightning proxy may performs better for shorter (i.e., subseasonal) climate timescales, especially
566 in the warm season. However, overall, ENSO and MJO spatial patterns of PR predicted lightning

567 look similar to the ENSO and MJO spatial patterns of observed lightning during 2003–2016 (cf.
568 Supplementary Figs. 1–4), suggesting that the PR model can capture large-scale, low-frequency
569 variability in lightning activity and is still useful in investigating climate links and patterns.

570 The lack of statistically significant MJO-lightning relations in our study is different from the
571 MJO-lightning patterns found in Abatzoglou and Brown (2009). Methodological differences may
572 play a role. Here, we demonstrated that failing to account for seasonality in MJO phase frequency
573 and lightning climatology resulted in type I errors (rejecting the null hypothesis when it is true)
574 in as many as 100% of cases. This behavior may provide an explanation for why the results here
575 differ from previous ones which did not take seasonality into consideration. The lack of a clear
576 relation between the MJO and lightning has implications for subseasonal prediction of lightning
577 activity and its indirect impacts (e.g., wildfire ignition).

578 Over the eastern U.S., the link between ENSO and lightning might be expected to be similar
579 to that between ENSO and severe convective storm activity. For instance, there is a documented
580 relationship between La Niña and increased frequency of tornado and hail events over the Tennessee
581 River Valley in late winter and early spring (Allen et al. 2015a; Koch et al. 2021; Tippett and Lepore
582 2021), which can be associated with ENSO-related CAPE patterns. However, the ENSO signals
583 in lightning are generally weaker than the ENSO signals in severe thunderstorms. We hypothesize
584 that the contrasting ENSO signals in CAPE and precipitation may be reducing the ENSO signal in
585 lightning, especially over the Tennessee River Valley. On the other hand, for severe thunderstorms,
586 additional environmental factors become relevant, such as storm relative helicity (SRH). ENSO
587 influences patterns of SRH and CAPE similarly i.e., La Niña increases both CAPE and SRH
588 in the region (Lepore et al. 2018; Koch et al. 2021), and the ENSO signal in SRH is stronger
589 than (convective) precipitation in climate forecast models, which can overpower any opposing
590 precipitation signals in the region.

591 The NLDN is one of the most reliable datasets of lightning observations available, but future work
592 should consider, when available, the re-classified NLDN data, which estimates 2015–2022 lightning
593 counts with improved detection methods (personal communications, Koshak 2023). Future work
594 should also consider how this PR model could be used to understand how other climate modes
595 of variability may influence lightning activity as well as for identifying trends. Global lightning
596 trends are not well understood, and there is general disagreement on whether lightning activity

597 will increase or decrease with a warming climate (Price and Rind 1994; Finney et al. 2018; Romps
598 2019). Some studies have reported that U.S. CG lightning has increased (Romps et al. 2014;
599 Romps 2019), including over the Great Plains where severe thunderstorms are frequent (Villarini
600 and Smith 2013). However, these studies use datasets with short records, so there would be benefit
601 from a comprehensive analysis over a longer period of time and over the entire U.S.

602 *Acknowledgments.* The authors gratefully acknowledge Vaisala Inc. for providing the NLDN data
603 used in this study as part of the Marshall Mentored Project (MMP, ID #02). The work by co-author
604 Koshak was supported by the Precipitation and Lightning Work Package for the Internal Science
605 Funding Model (ISFM) project Lightning as an Indicator of Climate under NASA Headquarters
606 (Dr. Jack Kaye and Dr. Lucia Tsaoussi), which supports NASA's participation in the National
607 Climate Assessment (NCA). The authors thank Paul E. Roundy and two anonymous reviewers for
608 their constructive feedback, which improved the paper.

609 *Data availability statement.* Proprietary NLDN data were provided by Vaisala Inc. and is available
610 for purchase at <https://www.vaisala.com/en/digital-and-data-services/lightning>.
611 NARR data are provided by the NOAA/OAR/ESRL PSD, Boulder, Colorado, USA from their
612 website <https://psl.noaa.gov/data/gridded/data.narr.html>. MJO RMM data are pro-
613 vided by the Centre for Australian Weather and Climate Research from their website [http://](http://www.bom.gov.au/climate/mjo/)
614 www.bom.gov.au/climate/mjo/. ONI data are provided by NOAA/CPC at [https://origin.](https://origin.cpc.ncep.noaa.gov/products/analysis_monitoring/ensostuff/ONI_v5.php)
615 [cpc.ncep.noaa.gov/products/analysis_monitoring/ensostuff/ONI_v5.php](https://origin.cpc.ncep.noaa.gov/products/analysis_monitoring/ensostuff/ONI_v5.php).

616 **References**

617 Abatzoglou, J. T., and T. J. Brown, 2009: Influence of the Madden–Julian oscillation on sum-
618 mertime cloud-to-ground lightning activity over the continental United States. *Monthly weather*
619 *review*, **137** (10), 3596–3601.

620 Allen, J. T., M. K. Tippett, and A. H. Sobel, 2015a: An empirical model relating US monthly hail
621 occurrence to large-scale meteorological environment. *Journal of Advances in Modeling Earth*
622 *Systems*, **7** (1), 226–243.

623 Allen, J. T., M. K. Tippett, and A. H. Sobel, 2015b: Influence of the El Niño/Southern Oscillation
624 on tornado and hail frequency in the United States. *Nature Geoscience*, **8** (4), 278–283.

- 625 Baggett, C. F., K. M. Nardi, S. J. Childs, S. N. Zito, E. A. Barnes, and E. D. Maloney, 2018: Skillful
626 subseasonal forecasts of weekly tornado and hail activity using the Madden-Julian Oscillation.
627 *Journal of Geophysical Research: Atmospheres*, **123** (22), 12–661.
- 628 Becker, E., H. v. den Dool, and Q. Zhang, 2014: Predictability and forecast skill in NMME. *Journal*
629 *of Climate*, **27** (15), 5891–5906.
- 630 Becker, E. J., E. H. Berbery, and R. W. Higgins, 2011: Modulation of cold-season US daily
631 precipitation by the Madden-Julian oscillation. *Journal of Climate*, **24** (19), 5157–5166.
- 632 Benjamini, Y., and Y. Hochberg, 1995: Controlling the false discovery rate: a practical and powerful
633 approach to multiple testing. *Journal of the Royal statistical society: series B (Methodological)*,
634 **57**, 289–300.
- 635 Biagi, C. J., K. L. Cummins, K. E. Kehoe, and E. P. Krider, 2007: National lightning detection
636 network (NLDN) performance in southern Arizona, Texas, and Oklahoma in 2003–2004. *Journal*
637 *of Geophysical Research: Atmospheres*, **112** (D5).
- 638 Branick, M. L., and C. A. Doswell III, 1992: An observation of the relationship between supercell
639 structure and lightning ground-strike polarity. *Weather and Forecasting*, **7** (1), 143–149.
- 640 Bukovsky, M. S., and D. J. Karoly, 2007: A brief evaluation of precipitation from the North
641 American Regional Reanalysis. *Journal of Hydrometeorology*, **8** (4), 837–846.
- 642 Camargo, S. J., M. K. Tippett, A. H. Sobel, G. A. Vecchi, and M. Zhao, 2014: Testing the
643 performance of tropical cyclone genesis indices in future climates using the HiRAM model.
644 *Journal of Climate*, **27** (24), 9171–9196.
- 645 Cui, W., X. Dong, B. Xi, and A. Kennedy, 2017: Evaluation of reanalyzed precipitation variability
646 and trends using the gridded gauge-based analysis over the CONUS. *Journal of Hydrometeorol-*
647 *ogy*, **18** (8), 2227–2248.
- 648 Cummins, K. L., and M. J. Murphy, 2009: An overview of lightning locating systems: History,
649 techniques, and data uses, with an in-depth look at the US NLDN. *IEEE transactions on*
650 *electromagnetic compatibility*, **51** (3), 499–518.

- 651 DelSole, T., L. Trenary, M. K. Tippett, and K. Pegion, 2017: Predictability of week-3–4 average
652 temperature and precipitation over the contiguous United States. *Journal of Climate*, **30** (10),
653 3499–3512.
- 654 DelSole, T. M., and M. K. Tippett, 2022: *Statistical Methods for Climate Scientists*. Cambridge
655 University Press, <https://doi.org/10.1017/9781108659055>.
- 656 Dewan, A., E. T. Ongee, M. Rafiuddin, M. M. Rahman, and R. Mahmood, 2018: Lightning activity
657 associated with precipitation and CAPE over Bangladesh. *International Journal of Climatology*,
658 **38** (4), 1649–1660.
- 659 Dowdy, A. J., 2016: Seasonal forecasting of lightning and thunderstorm activity in tropical and
660 temperate regions of the world. *Scientific reports*, **6** (1), 1–10.
- 661 Fierro, A. O., E. R. Mansell, D. R. MacGorman, and C. L. Ziegler, 2013: The implementation of
662 an explicit charging and discharge lightning scheme within the WRF-ARW model: Benchmark
663 simulations of a continental squall line, a tropical cyclone, and a winter storm. *Monthly Weather*
664 *Review*, **141** (7), 2390–2415.
- 665 Finney, D. L., R. M. Doherty, O. Wild, D. S. Stevenson, I. A. MacKenzie, and A. M. Blyth, 2018:
666 A projected decrease in lightning under climate change. *Nature Climate Change*, **8** (3), 210–213.
- 667 Fuchs, B. R., and Coauthors, 2015: Environmental controls on storm intensity and charge struc-
668 ture in multiple regions of the continental United States. *Journal of Geophysical Research:*
669 *Atmospheres*, **120** (13), 6575–6596.
- 670 Gensini, V. A., T. L. Mote, and H. E. Brooks, 2014: Severe-thunderstorm reanalysis environments
671 and collocated radiosonde observations. *Journal of Applied Meteorology and Climatology*,
672 **53** (3), 742–751.
- 673 Goodman, S. J., and D. R. MacGorman, 1986: Cloud-to-ground lightning activity in mesoscale
674 convective complexes. *Monthly Weather Review*, **114** (12), 2320–2328.
- 675 Holle, R. L., K. L. Cummins, and W. A. Brooks, 2016: Seasonal, monthly, and weekly distributions
676 of NLDN and GLD360 cloud-to-ground lightning. *Monthly Weather Review*, **144** (8), 2855–
677 2870.

678 Jung, E., and B. P. Kirtman, 2016: Can we predict seasonal changes in high impact weather in the
679 United States? *Environmental Research Letters*, **11** (7), 074 018.

680 Kang, D., R. Mathur, G. A. Pouliot, R. C. Gilliam, and D. C. Wong, 2020: Significant ground-level
681 ozone attributed to lightning-induced nitrogen oxides during summertime over the mountain
682 west states. *NPJ climate and atmospheric science*, **3** (1), 1–7.

683 Kim, D., S.-K. Lee, and H. Lopez, 2020: Madden–Julian oscillation–induced suppression of
684 northeast Pacific convection increases US tornadogenesis. *Journal of Climate*, **33** (11), 4927–
685 4939.

686 King, A. T., and A. D. Kennedy, 2019: North American supercell environments in atmospheric
687 reanalyses and RUC-2. *Journal of Applied Meteorology and Climatology*, **58** (1), 71–92.

688 Koch, E., J. Koh, A. C. Davison, C. Lepore, and M. K. Tippett, 2021: Trends in the extremes of
689 environments associated with severe US thunderstorms. *Journal of Climate*, **34** (4), 1259–1272.

690 Koehler, T. L., 2020: Cloud-to-ground lightning flash density and thunderstorm day distributions
691 over the contiguous United States derived from NLDN measurements: 1993–2018. *Monthly*
692 *Weather Review*, **148** (1), 313–332.

693 Koshak, W. J., K. L. Cummins, D. E. Buechler, B. Vant-Hull, R. J. Blakeslee, E. R. Williams,
694 and H. S. Peterson, 2015: Variability of CONUS lightning in 2003–12 and associated impacts.
695 *Journal of Applied Meteorology and Climatology*, **54** (1), 15–41.

696 Laing, A., M. LaJoie, S. Reader, and K. Pfeiffer, 2008: The influence of the El Niño–Southern
697 Oscillation on cloud-to-ground lightning activity along the Gulf Coast. Part II: Monthly corre-
698 lations. *Monthly Weather Review*, **136** (7), 2544–2556.

699 LaJoie, M., and A. Laing, 2008: The influence of the El Niño–Southern Oscillation on cloud-to-
700 ground lightning activity along the Gulf Coast. Part I: Lightning climatology. *Monthly Weather*
701 *Review*, **136** (7), 2523–2542.

702 Lepore, C., M. K. Tippett, and J. T. Allen, 2018: CFSv2 monthly forecasts of tornado and hail
703 activity. *Weather and Forecasting*, **33** (5), 1283–1297.

- 704 Lynn, B. H., Y. Yair, C. Price, G. Kelman, and A. J. Clark, 2012: Predicting cloud-to-ground and
705 intracloud lightning in weather forecast models. *Weather and Forecasting*, **27 (6)**, 1470–1488.
- 706 L'Heureux, M. L., M. K. Tippett, and A. G. Barnston, 2015: Characterizing ENSO coupled
707 variability and its impact on North American seasonal precipitation and temperature. *Journal of*
708 *Climate*, **28 (10)**, 4231–4245.
- 709 MacGorman, D. R., and D. W. Burgess, 1994: Positive cloud-to-ground lightning in tornadic
710 storms and hailstorms. *Monthly Weather Review*, **122 (8)**, 1671–1697.
- 711 Mansell, E. R., D. R. MacGorman, C. L. Ziegler, and J. M. Straka, 2005: Charge structure and
712 lightning sensitivity in a simulated multicell thunderstorm. *Journal of Geophysical Research:*
713 *Atmospheres*, **110 (D12)**.
- 714 McCaul, E. W., S. J. Goodman, K. M. LaCasse, and D. J. Cecil, 2009: Forecasting lightning threat
715 using cloud-resolving model simulations. *Weather and Forecasting*, **24 (3)**, 709–729.
- 716 Medici, G., K. L. Cummins, D. J. Cecil, W. J. Koshak, and S. D. Rudlosky, 2017: The intracloud
717 lightning fraction in the contiguous United States. *Monthly Weather Review*, **145 (11)**, 4481–
718 4499.
- 719 Mesinger, F., and Coauthors, 2006: North American regional reanalysis. *Bulletin of the American*
720 *Meteorological Society*, **87 (3)**, 343–360.
- 721 Michalon, N., A. Nassif, T. Saouri, J. Royer, and C. Pontikis, 1999: Contribution to the climato-
722 logical study of lightning. *Geophysical research letters*, **26 (20)**, 3097–3100.
- 723 Moore, T. W., and M. P. McGuire, 2020: Tornado-days in the United States by phase of the
724 Madden–Julian oscillation and global wind oscillation. *Climate Dynamics*, **54 (1-2)**, 17–36.
- 725 Mülmenstädt, J., O. Sourdeval, J. Delanoë, and J. Quaas, 2015: Frequency of occurrence of rain
726 from liquid-, mixed-, and ice-phase clouds derived from A-Train satellite retrievals. *Geophysical*
727 *Research Letters*, **42 (15)**, 6502–6509.
- 728 Muñoz, Á., J. Díaz-Lobato, X. Chourio, and M. Stock, 2016: Seasonal prediction of lightning
729 activity in north western Venezuela: Large-scale versus local drivers. *Atmospheric Research*,
730 **172**, 147–162.

731 Murugavel, P., S. Pawar, and V. Gopalakrishnan, 2012: Trends of convective available potential
732 energy over the Indian region and its effect on rainfall. *International Journal of Climatology*,
733 **32 (9)**, 1362–1372.

734 Nag, A., M. J. Murphy, and J. A. Cramer, 2016: Update to the US national lightning detection
735 network. *24th International Lightning Detection Conference and 6th International Lightning*
736 *Meteorology Conference*.

737 Nigam, S., and A. Sengupta, 2021: The full extent of El Niño’s precipitation influence on the
738 United States and the Americas: The suboptimality of the Niño 3.4 SST index. *Geophysical*
739 *Research Letters*, **48 (3)**, e2020GL091447.

740 Pegion, K., and Coauthors, 2019: The Subseasonal Experiment (SubX): A multimodel subseasonal
741 prediction experiment. *Bulletin of the American Meteorological Society*, **100 (10)**, 2043–2060.

742 Petersen, W. A., and S. A. Rutledge, 1998: On the relationship between cloud-to-ground lightning
743 and convective rainfall. *Journal of Geophysical Research: Atmospheres*, **103 (D12)**, 14 025–
744 14 040.

745 Price, C., and D. Rind, 1994: Possible implications of global climate change on global lightning
746 distributions and frequencies. *Journal of Geophysical Research: Atmospheres*, **99 (D5)**, 10 823–
747 10 831.

748 Romps, D. M., 2019: Evaluating the future of lightning in cloud-resolving models. *Geophysical*
749 *Research Letters*, **46 (24)**, 14 863–14 871.

750 Romps, D. M., A. B. Charn, R. H. Holzworth, W. E. Lawrence, J. Molinari, and D. Vollaro,
751 2018: CAPE times P explains lightning over land but not the land-ocean contrast. *Geophysical*
752 *Research Letters*, **45 (22)**, 12–623.

753 Romps, D. M., J. T. Seeley, D. Vollaro, and J. Molinari, 2014: Projected increase in lightning
754 strikes in the United States due to global warming. *Science*, **346 (6211)**, 851–854.

755 Saha, S., and Coauthors, 2014: The NCEP climate forecast system version 2. *Journal of climate*,
756 **27 (6)**, 2185–2208.

757 Stainforth, D. A., M. R. Allen, E. R. Tredger, and L. A. Smith, 2007: Confidence, uncertainty
758 and decision-support relevance in climate predictions. *Philosophical Transactions of the Royal*
759 *Society A: Mathematical, Physical and Engineering Sciences*, **365 (1857)**, 2145–2161.

760 Stolz, D. C., S. A. Rutledge, J. R. Pierce, and S. C. van den Heever, 2017: A global lightning
761 parameterization based on statistical relationships among environmental factors, aerosols, and
762 convective clouds in the TRMM climatology. *Journal of Geophysical Research: Atmospheres*,
763 **122 (14)**, 7461–7492.

764 Thompson, D. B., and P. E. Roundy, 2013: The relationship between the Madden–Julian oscillation
765 and US violent tornado outbreaks in the spring. *Monthly Weather Review*, **141 (6)**, 2087–2095.

766 Tippett, M. K., 2018: Robustness of relations between the MJO and US tornado occurrence.
767 *Monthly Weather Review*, **146 (11)**, 3873–3884.

768 Tippett, M. K., and W. J. Koshak, 2018: A baseline for the predictability of US cloud-to-ground
769 lightning. *Geophysical Research Letters*, **45 (19)**, 10–719.

770 Tippett, M. K., and C. Lepore, 2021: ENSO-based predictability of a regional severe thunderstorm
771 index. *Geophysical Research Letters*, **48 (18)**, e2021GL094 907.

772 Tippett, M. K., C. Lepore, W. J. Koshak, T. Chronis, and B. Vant-Hull, 2019: Performance of a
773 simple reanalysis proxy for US cloud-to-ground lightning. *International Journal of Climatology*,
774 **39 (10)**, 3932–3946.

775 Villarini, G., and J. A. Smith, 2013: Spatial and temporal variability of cloud-to-ground lightning
776 over the continental US during the period 1995–2010. *Atmospheric research*, **124**, 137–148.

777 Virts, K. S., and R. A. Houze, 2015: Variation of lightning and convective rain fraction in mesoscale
778 convective systems of the MJO. *Journal of the Atmospheric Sciences*, **72 (5)**, 1932–1944.

779 Vitart, F., and Coauthors, 2017: The subseasonal to seasonal (S2S) prediction project database.
780 *Bulletin of the American Meteorological Society*, **98 (1)**, 163–173.

781 Westermayer, A., P. Groenemeijer, G. Pistotnik, R. Sausen, and E. Faust, 2017: Identification of
782 favorable environments for thunderstorms in reanalysis data. *Meteorologische Zeitschrift*, **26 (1)**,
783 59–70.

- 784 Wheeler, M. C., and H. H. Hendon, 2004: An all-season real-time multivariate MJO index:
785 Development of an index for monitoring and prediction. *Monthly Weather Review*, **132 (8)**,
786 1917–1932.
- 787 Wilks, D., 2016: “The stippling shows statistically significant grid points”: How research results
788 are routinely overstated and overinterpreted, and what to do about it. *Bulletin of the American*
789 *Meteorological Society*, **97 (12)**, 2263–2273.
- 790 Xu, W., R. F. Adler, and N.-Y. Wang, 2013: Improving geostationary satellite rainfall estimates using
791 lightning observations: Underlying lightning–rainfall–cloud relationships. *Journal of applied*
792 *meteorology and climatology*, **52 (1)**, 213–229.
- 793 Yair, Y., B. Lynn, C. Price, V. Kotroni, K. Lagouvardos, E. Morin, A. Mugnai, and M. d. C.
794 Llasat, 2010: Predicting the potential for lightning activity in Mediterranean storms based on
795 the Weather Research and Forecasting (WRF) model dynamic and microphysical fields. *Journal*
796 *of Geophysical Research: Atmospheres*, **115 (D4)**.
- 797 Zajac, B. A., and S. A. Rutledge, 2001: Cloud-to-ground lightning activity in the contiguous
798 United States from 1995 to 1999. *Monthly Weather Review*, **129 (5)**, 999–1019.
- 799 Zhao, P., H. Xiao, C. Liu, Y. Zhou, X. Xu, and K. Hao, 2022: Evaluating a simple proxy for
800 climatic cloud-to-ground lightning in Sichuan Province with complex terrain, Southwest China.
801 *International Journal of Climatology*, **42 (7)**, 3909–3927.
- 802 Zipser, E. J., 1994: Deep cumulonimbus cloud systems in the tropics with and without lightning.
803 *Monthly weather review*, **122 (8)**, 1837–1851.